

The Optical/Infrared Astronomical Quality of High Atacama Sites. I. Preliminary Results of Optical Seeing

Riccardo Giovanelli¹, Jeremy Darling¹, Marc Sarazin², Jennifer Yu⁴, Paul Harvey³, Charles Henderson¹, William Hoffman¹, Luke Keller¹, Don Barry¹, James Cordes¹, Stephen Eikenberry¹, George Gull¹, Joseph Harrington¹, J. D. Smith¹, Gordon Stacey¹, Mark Swain¹

¹Department of Astronomy, Cornell University, Ithaca, NY 14853

²European Southern Observatory, Garching bei München, D-85748 Germany

³Department of Astronomy, University of Texas, Austin, TX 78712

⁴Department of Earth and Atmospheric Sciences, Cornell University, Ithaca, NY 14853

ABSTRACT

The region surrounding the Llano de Chajnantor, a high altitude plateau in the Atacama Desert in northern Chile, has caught the attention of the astronomical community for its potential as an observatory site. Combining high elevation and extremely low atmospheric water content, the Llano has been chosen as the future site of the Atacama Large Millimeter Array. We have initiated a campaign to investigate the astronomical potential of the region in the optical/infrared. Here, we report on an aspect of our campaign aimed at establishing a seeing benchmark to be used as a reference for future activities in the region. After a brief description of the region and its climate, we describe the results of an astronomical seeing campaign, carried out with a Differential Image Motion Monitor that operates at 0.5 μm wavelength. The seeing at the Llano level of 5000 m, measured over 7 nights in May 1998, yielded a median FWHM of 1.1". However, the seeing decreased to 0.7" at a modest 100 m gain above the plateau (Cerro Chico), as measured over 38 nights spread between July 1998 and October 2000. Neither of these represents the best seeing expected in the region; the set of measurements provides a reference base for simultaneous dual runs at Cerro Chico and at other sites of interest in the region, currently underway. A comparison between simultaneous measurements at Cerro Chico and Cerro Paranal indicates that seeing at Cerro Chico is about 12% better than at Paranal. The percentage of optically photometric nights in the Chajnantor region is about 60%, while that of nights useful for astronomical work is near 80%.

Subject Headings: Astronomical instrumentation, methods and techniques: atmospheric effects, site testing.

1. Introduction

Outer space provides the ideal setting for astronomical instruments. Freeing them from the limitations imposed by our planet’s atmosphere, observations of high angular resolution and in spectral bands to which the atmosphere is opaque have become possible. However, because of the steep costs of hauling large masses to space, very large collecting area telescopes have remained the domain of ground-based observatories. In addition to high sensitivity, large apertures, aided by adaptive optics techniques, allow high angular resolution images to be obtained from the ground, which are most effective in sites with good astronomical seeing. Especially in the infrared, atmospheric opacity and emissivity can be minimized by placing observatories at high altitude or in extremely cold locations. The South Pole has witnessed strong growth in the number and quality of astronomical installations in recent years. Similarly, high and dry sites have become increasingly attractive, in spite of the operational difficulties that arise with high altitude.

The Atacama Desert in northern Chile is one of the driest regions on Earth. It lies between the Coastal Cordillera to the west and the Andes to the east. The region of the Altiplano to the east of the Salar de Atacama known as Llano de Chajnantor, a plateau of altitude near 5000 m, was selected by the U.S. National Radio Astronomy Observatory (NRAO) as the future site for its Millimeter Array Project, while a neighboring plateau, *Pampa La Bola*, was selected by the Nobeyama Radio Observatory of Japan for its Large Millimeter and Submillimeter Array (LMSA) Project. These sites are within a few km from each other, at elevations between 4800 and 5050 m above mean sea level. Successively, the Millimeter Array Project has evolved into a U.S.–Europe consortium to build the Atacama Large Millimeter Array (ALMA). Other radio and optical Astronomy consortia are under development for operation in this region, which has the potential for expanding into a major world astronomical center. Cerro Paranal, the site of the European Southern Observatory’s (ESO) Very Large Telescope Project, is about 300 km to the southwest, on a peak on the Pacific coastal range (Coastal Cordillera).

The climatic qualities that make the Atacama region especially attractive to astronomers extend over a latitudinal band a few hundred kilometers wide, about the Tropic of Capricorn. The access to good quality services and good communications further focuses attention on the regions in the vicinity of the cities of Antofagasta, Calama and the village of San Pedro de Atacama. The presence of the VLT and the likely establishment of major national and international research centers, such as ALMA and the LMSA, adds promise of scientific and operational synergism to the region. The government of Chile has legislated the protection of an area which includes the Llano de Chajnantor, the Pampa La Bola and the surrounding peaks, as a *National Science Preserve*.

Several institutions are carrying out measurements to ascertain the characteristics of the region for astronomical observations in the radio and submillimeter parts of the spectrum. We have initiated a campaign to characterize the region for optical and infrared astronomical observations. In the following two sections, we present a brief description of the region and its climate. In Section 4, the seeing measurements and synoptic results are described, followed by brief remarks

on photometric conditions. We conclude with a discussion on plans and prospects for future work. In a companion paper (Giovanelli *et al.* 2001; Paper II), we present the results of measurements regarding the water vapor content and its implications on infrared transparency and background emissivity.

2. Description of the Region

The Salar de Atacama ($23^{\circ} 30' S$, $68^{\circ} 15' W$) is the largest salt flat in Chile. A basin with median elevation near 2300 m, it extends for more than 100 km from north to south, lies 200 km inland from the Pacific coast and is located about 1600 km north of the capital city of Santiago. The Salar is bounded to the west by the Domeyko mountain range, with peaks as high as 4300 m (Cerro Quimal), and to the east by the main Andean magmatic arc. Among the highest Andean peaks in the vicinity are Llullaillaco (6723 m) south of the Salar, and Acamarachi or Pili (6046 m), while among the most spectacular are Licancabur (5950 m) and Láscaar (5592 m). Figure 1 is a composite satellite image of a region of approximately 400 by 200 km, extending from the Pacific coast on the west to the Andes on the east. The image is the combination of three frames taken through different broad-band filters: $0.5 \mu\text{m}$ (blue), $1.0 \mu\text{m}$ (green) and $1.5 \mu\text{m}$ (red). Data were acquired on July 20, 1985 by the Landsat 5 imaging satellite. The Salar de Atacama is the region filled with muds and evaporitic deposits outlined in light brown to the right and below of center, bordered on its right by turquoise hues (salt deposits and ponded water). To the east, where the volcanoes of the Andean magmatic arc rise above 5000 m, moisture has been intercepted by the high peaks and precipitated as snow on the plateau (represented by bright blue). The city of Antofagasta is to the south of the anvil-shaped Mejillones Peninsula, at the lower left in the figure.

Around the Salar, human settlements are only found in the vicinity of oases and they are generally quite small. The largest among them includes the village of San Pedro and its environs, with a combined population of about 1,200. San Pedro is located at the northern end of the Salar de Atacama, just to the west (left) of the red outline in Figure 1. No humans reside between San Pedro and the Bolivian border, 50 km to the northeast, nor between San Pedro and the Argentine border, 160 km to the east. The nearest large urban center is Calama–Chuquicamata, with a combined population of about 150,000, 100 km to the northwest of San Pedro, beyond the Domeyko range. Calama–Chuquicamata is at the center of the most important copper mining zone in the South American continent (just south of the upper boundary, center, of the image in Figure 1). Its airport is connected by several daily flights to other Chilean cities, such as Antofagasta, Santiago, Copiapó and La Serena. Antofagasta, the regional capital with a population of one-third of a million, is on the coast 200 km to the west of Calama. The nearest town with population exceeding 1000 to the east of San Pedro is across the Andes, some 500 km away. To the north, the nearest settlements are at Ollagüe, at 300 km, and Uyuni, 400 km away; neither exceeds the size of San Pedro. To the south, only a few villages much smaller than San Pedro dot the edges of the Salar. From an urban viewpoint, Atacama is thus a region of extreme isolation.

Traffic is however increasing, both because the colonial and archaeological patrimony and natural beauty of the surroundings make San Pedro a favorite tourist destination, and because the international Andean road through the Paso de Jama to Argentina is now paved. This road will likely become one of the main arteries between the continental heartland (northern Argentina, Paraguay and southern Brazil) and the Pacific Ocean. The use of urban lights will undoubtedly increase in San Pedro. However, the likelihood of tumultuous future development of San Pedro or of any of the neighboring villages into major desert centers, as has occurred in the American Southwest, is remote. Sizable sources of water in the region are absent. In spite of the high altitude of the Andean peaks, there are no extensive glaciers in this region, and precipitation is extremely rare. The villages in the Atacama Desert are unlikely to pose a serious light pollution threat in the foreseeable future.

The quality of services in the region is high, a result of the conspicuous presence of major mining interests. Roads are good, supply, communications and financial services are excellent, medical services abound and unique expertise in the special circumstances of high altitude physiology exists. For example, delivery of supplies, from water to cryogenics, to remote, high altitude sites is a routine practice; engineering contracting companies expert in planning and construction of facilities at high altitude are numerous; and international meetings on high altitude medicine are held in the region (e.g. Iquique, November 2000).

The Llano de Chajnantor is located about 40 km to the east of San Pedro, and nearly 3000 m higher in elevation. The region is illustrated in Figure 2, an area of 1560 km² roughly corresponding to that within the box outline in Figure 1. The Salar de Atacama lies to the southwest of the region displayed in Figure 2 and the town of San Pedro is at the northern end of the Salar, about one half map-width off the western margin of the map. Several notable features are labeled. The two volcanoes *Licancabur* (5950 m) and *Juriques* (5750 m, with the red-rimmed crater) are in the northwest. Licancabur (label 10), is a prominent, symmetric cone and marks the southwestern vertex of the Chile–Bolivia political border. To the northeast of the two volcanoes are the two lagoons jointly known as *Laguna Verde*, in Bolivian territory. Near the center is *Cerro Chajnantor* (label 5, 5700 m); to the southeast of it is *Cerro Chascón* (label 6, 5750 m) and to the northeast is *Cerro Toco* (label 7, 5650 m). A sulphur-rich ground surface, east of Toco’s summit, is responsible for the white coloring in that part of the image. Light blue implies the presence of snow. The red-colored ridge running northeast to southwest (label 4), is known as *Cerros de Honar* (5400 m), and the mountain labeled 8 is *Cerro Negro* (5100 m). The chain of hills separating Negro and Honar are known as *Cerros de Macón* (5000 m). The Llano de Chajnantor is the area between Chajnantor, Chascón, Honar and Negro. Its average elevation is 5000 m. Both NRAO and ESO maintain ALMA site testing equipment in the plateau, at the location identified by the label 2 in the map. The region north of Chascón and east of Chajnantor is known as *Pampa La Bola*. At an average elevation of 4800 m, it hosts testing equipment of the Nobeyama Radio Observatory for the LMSA project, of Japan, near the label ‘9’. Finally, label ‘1’ identifies *Cerro Chico* (5150 m), the site at which most of the seeing tests described in this report were conducted; and label ‘3’

identifies the location of the radiosonde launch facility, jointly operated by Cornell, NRAO, ESO, the Harvard–Smithsonian Astrophysical Observatory (SAO) and the Nobeyama Radio Observatory (since 2000), which produced much of the atmospheric water vapor data discussed in Paper II.

For scale, the distance between the summits of Juriques and Chajnantor is 17.5 km. The study area is dominated by volcanic surfaces that range in age from approximately 10^6 to 10^7 years. These features are remarkably well-preserved due to the aridity of the region. The Llano de Chajnantor is part of a circular area about 12 km in diameter centered on Cerro Chajnantor, which is a Quaternary andesitic dome. The surrounding surfaces include Plio-Quaternary andesites and Quaternary ignimbrites. The drainages lead radially outward from Cerro Chajnantor. The topography rapidly loses elevation moving 30 km west from the edge of the Llano at 5000 m to the Salar at 2300 m. Among the peaks in the area, Honar rises 400 m above the plateau, Chico rises less than 150 m, Chajnantor and Toco both rise about 650 m, and Chascón is the highest local point at 800 m above the Llano. Images of the region can be viewed at <http://www.astro.cornell.edu/atacama>.

The northern Chilean Andes include a high concentration of geologically active volcanoes. In the vicinity of Chajnantor, the only conspicuous and current activity takes place at Volcán Láscar, located about 30 km south of Honar. Láscar’s last mayor eruption took place in 1993, producing a tephra cloud which the winds carried principally eastward. It produced volcanic ash deposits 3 cm thick 50 km downwind from its crater (González–Ferrán 1994). A minor eruption of the same volcano took place on July 20, 2000, during one of our campaign runs. The likelihood of other volcanic eruptions in the region are discussed by Gardeweg (1996), while a thorough survey of the volcanology in Chile is given by González–Ferrán (1994).

3. Remarks on Climate

3.1. Conditions at the Llano de Chajnantor

The work of Dieter Schmidt (1996) provides the most recent and complete compendium of climatological conditions of the Atacama. See also Cook (2000) and Fuenzalida (1984).

The large-scale climatological patterns of the region are associated with the persistence of the Southeast Pacific subtropical anticyclone. An important driving force of the regional weather pattern is the extremely high fraction of the solar radiation flux reaching the ground, due to the tropical location and the high atmospheric transparency. The heat input by radiation is released through convective and advective processes, due to the lack of humidity to form latent heat, with the wind playing an important role in heat transport. Low altitude winds in this region are generally driven by the temperature differences between the Pacific coast and the Andean region, exhibiting a clear diurnal cycle. Both the diurnal and seasonal cycles of the wind speed at the Llano de Chajnantor, as recorded at the ALMA site between 1995 and 2000, can be viewed in the composite figures of the continuously updated NRAO web site <http://www.tuc.nrao.edu/mma/sites/Chajnantor/data.c.html>

(Radford 2000).

Between April 1995 and October 2000, the 25%, 50% and 75% wind speed quartiles were respectively 3.1, 6.4 and 10.3 m s⁻¹ at the plateau level. Higher speeds occur during daytime hours, rising rapidly a few hours after sunrise in mid-winter and in the mid-afternoon during Summer. Sustained speeds can exceed 15 m s⁻¹. The nighttime median wind speed at 4 meters off the ground is about 4 m s⁻¹, a relatively benign condition which is, in fact, lower than that observed at Mauna Kea. In both Summer and Winter, wind speed drops precipitously about one or two hours after sunset. A seasonal pattern is also clear, with wind speeds decreasing in the austral Summer months. Wind direction is also tied to the seasonal cycle: the flow is nearly always from the west between April and early December, while the wind direction becomes more variable in the Summer months, when conditions locally referred to as “Bolivian Winter” often ensue. These are associated with the inflow of moist Amazonic air from the NE. Hence the local name. Wind storms lasting 1–2 days with wind speeds exceeding 25 m s⁻¹ occur a few times per year, especially during winter months. These events are well correlated with high wind speeds at the 200 mb level, the occurrence of which can be anticipated several days in advance with good reliability. In that respect, the forecasts posted by M. Sarazin in <http://www.eso.org/gen-fac/pubs/astclim/forecast/meteo/ECMWF/long/chajnantor> have proved extremely valuable for our campaign activities.

High winds can be of hindrance to astronomical operation not only because of their mechanical effects, but also because they can increase the density of dust found in suspension in the atmosphere. Near valley floors, in fact, dust storms are frequent, due to the sandy characteristics of the soil. In the Chajnantor region, however, the ground is generally a mixture of rock and gravel, and little dust is raised even by the strong daytime winds. The valley dust layer is seldom seen to rise above the 4500 m level. Quantitative determinations of atmospheric dust content at Chajnantor are planned.

The ground temperature distribution at the Llano de Chajnantor, as recorded at the ALMA site testing station, can also be appreciated in Radford (2000) both in its seasonal and diurnal characteristics. The historical 25%, 50% and 75% quartile values for ground level temperature at the ALMA monitoring site are respectively 2.9 C, -2.6 C and -7.8 C. The diurnal cycle has an amplitude of 13–14 C, while the seasonal cycle has a slightly lesser amplitude of 10–12 C. The temperatures at the plateau are not extreme, reaching as high as 15 C during summer days and seldom falling below -15 C during winter nights. Night temperatures vary little: between 0 and 10 hours UT (approximately 7:30 p.m. and 5:30 a.m., local time), the average temperature drop is 2.5 C, i.e. approximately 0.25 C hr⁻¹.

At San Pedro de Atacama, precipitation is extremely low, typically 50 mm or less per year. At the plateau it precipitates somewhat more frequently, generally in the form of snow and more likely when Bolivian Winter conditions occur. Snow accumulation seldom exceeds a few cm, although wind-driven drifts may accumulate layers of substantial thickness in sheltered depressions of the terrain. In shaded areas, melting and sublimation is slow and relatively small amounts of snow can last weeks or months.

El Niño–La Niña events, of 12 to 24 months duration, produce very significant alterations, superimposed on the annual cycle of atmospheric conditions. Severe *El Niño* events recur about once per decade, based on records of the last two centuries, while more moderate events take place about twice as frequently (Rodbell *et al.* 1999; see Neelin & Latif 1998 for a recent description of El Niño dynamics). The last *El Niño–La Niña* event took place between December 1997 and late 1998. It is reported to have been among the most severe since the middle of the XIX century (McPhaden 1999). During this event, the sea surface temperature anomaly in equatorial waters approached 5 C, while the average event produces deviations of 1.5 C or less. The effects of the 1997–98 episode resulted in higher humidity, increased atmospheric opacity and worse seeing conditions than normal, as we discuss later.

3.2. The Mean Atmosphere Above the Llano de Chajnantor

Since sites above the plateau will provide the best conditions for optical/IR telescopes, it is important to know what the differential meteorological conditions are between the relatively well sampled plateau level and the higher elevations. Continuous monitoring of the meteorological parameters at elevations above the Llano de Chajnantor has only started in October 2000, thus no reliable record exists of the differential conditions among sites. Some indications of the conditions that might be expected at higher elevations can however be garnered from radiosonde launches that have taken place since 1998, as we report elsewhere in greater detail (Paper II). In this Section, we restrict our presentation to median atmospheric profiles obtained from 106 radiosonde launches.

We have selected 30 sondes launched in nighttime hours (UT 01 to 11 hours; local midnight takes place at 04^h 31^m) and 65 sondes launched in daytime hours (UT 12 to 21 hrs). The sondes were launched between the months of April and early December, although the month of November is overrepresented (14 of 30 night launches and 25 of 65 day launches); thus they are representative of Winter and Spring, which is the period when the best astronomical observing conditions are found in the region.

The median atmospheric profiles these data yield are very instructional. Profiles are averaged over intervals of 10 m in altitude and shown in Figures 3 and 4, It should be kept in mind that these profiles refer to the free atmosphere and, due to prevailing winds, generally the sonde flights sample an inclined path that takes them to the east of the plateau. Conditions may thus be slightly different than over the Llano de Chajnantor proper. In addition, conditions at the peaks of mountains may be slightly different from those of the free atmosphere, as they will be affected by local topography. Nonetheless, these mean profiles give us at least a rough idea of the conditions we may encounter at various sites above the plateau.

Figure 3 indicates that at night there is a conspicuous inversion layer near the ground, which is at an elevation of 5000 m. The air temperature increases by several degrees up to about 100 m above the ground. This is a consequence of the rapid radiative cooling of the ground after sunset.

Between 5100 and 6000 m, the median temperature profile is ragged, due to the frequent occurrence of temperature inversions. Above 6 km elevation, a closer to normal tropospheric cooling trend with altitude takes over, at a rate of about 0.7 C per 100 m, somewhat lower than the adiabatic lapse rate of 0.98 C per 100 m. Conditions at peaks a few hundred meters above the plateau will not be harshly different than conditions at the plateau itself. The lapse rate during daytime is steeper in the lower 500 m, but median Winter temperatures above -10 C can be expected at all accessible ground sites. Quartile profiles (dotted lines) in Figure 3 refer to nighttime.

Figure 4 illustrates the median wind profile. Day and night data show, overall, similar profiles from an altitude of 6 km up, the wind speed increasing from about 10 m s⁻¹ at 6 km to about 25 m s⁻¹ at 12 km. Differences are most important near the ground, especially between 5 and 6.5 km altitude. During day time, the median wind speed at the ground is 7–8 m s⁻¹; it increases to about 10 m s⁻¹ by 5.3 km, and to 12 m s⁻¹ by 6.0 km. The night time profile is steeper. It rises from about 4 m s⁻¹ near the ground to about 8 m s⁻¹ at altitude 5.3 km, then hovers near 10–11 m s⁻¹ up to 6.2 km. The wind speed at any peak fully exposed to the free atmosphere should not be any less than the free atmosphere wind shown in Figure 4. Thus, night time wind speeds at Cerro Honar (5400 m) should be expected near 8 m s⁻¹, or twice as high as those at the plateau level, while at higher peaks such as Toco, Chajnantor and Chascón, mean speeds of the order of 10 m s⁻¹ should be expected. Actual wind speeds will depend critically on the characteristics of the air flow and the local topography. The profile of the 75% quartile of night data does however indicate that most of the time median wind speeds should not exceed 12–15 m s⁻¹. Such wind speeds are usually considered to be safely within operational limits at modern observatories, although direct testing of gusting conditions is necessary.

4. Seeing

4.1. Definitions and Terminology

Astronomical seeing is the distortion of the radiation wavefront of a cosmic source, produced by variations in the index of refraction of air. In conditions that are conducive to astronomical observations, pressure and water vapor fluctuations are negligible, thus variations in the index of refraction result primarily from thermal fluctuations associated with turbulent air flow. The *temperature structure function* of an atmospheric layer at altitude h above the ground is defined in the form of a covariance

$$D_T(r, h) = \langle \Delta T(r, h)^2 \rangle \quad (1)$$

where $\Delta T(r, h)$ is the temperature difference between two points separated by a distance r , at constant altitude. Over a wide range of scales — between a minimum of a few mm below which turbulence is damped out and a maximum size of km, at which turbulence is injected for example by flow past an obstacle such as a mountain range — within the framework of Kolmogorov’s treatment

D_T is generally described by a power law of the form

$$D_T(r) \propto r^\beta \quad (2)$$

where $\beta \simeq 2/3$ (Tatarski 1961). The proportionality in equation 2 is mediated by the scale-independent *temperature structure parameter* (Roddier 1981):

$$C_T^2(h) = \frac{D_T(r)}{r^{2/3}} \quad (3)$$

which relates to the *refractive index structure parameter* via

$$C_n^2(h) = C_T^2(h) [80 \times 10^{-6} P(h)/T^2(h)]^2 \quad (4)$$

where the units of C_n^2 , pressure $P(h)$ and temperature $T(h)$ are respectively $\text{m}^{-2/3}$, mb and K.

The spatial coherence scale of atmospheric turbulence is expressed by the *Fried parameter* r_o (in m):

$$r_o = \left[0.423 k^2 \sec(ZA) \int_{h_o}^{\infty} C_n^2(h) dh \right]^{-3/5} \quad (5)$$

where k is the wavenumber in m^{-1} , ZA the zenith angle of the line of sight and h_o the elevation of the telescope above the ground in m.

Finally, the full-width at half-maximum of a stellar image at a wavelength λ is

$$\theta_{fwhm} = 0.98 \frac{\lambda}{r_o} \quad (6)$$

In other words, for a telescope of diameter D turbulence degrades the image resolution from $\theta_{diff} \simeq \lambda/D$ to the diffraction limit which would be observed with a telescope of aperture r_o , i.e. $\theta_{fwhm} \simeq \lambda/r_o$. Since $r_o \propto k^{-6/5}$, as indicated by Equation 5, and $\lambda = 2\pi/k$, then

$$\theta_{fwhm} \propto \lambda^{-0.2} \quad (7)$$

All layers of the atmosphere contribute to seeing, as illustrated by Equation 5. Turbulence originating in the telescope enclosure is referred to as *dome seeing*. In our site survey measurements, dome seeing, as well as that arising from temperature differences between the mirror and the air, are null as our telescope has extremely small thermal capacity and it operates outdoors. The seeing that originates from convective flows between the ground and the few meters above it, and by turbulence arising from air flow between observatory buildings, is generally referred to as *ground surface layer seeing*. Seeing that originates from large scale interactions between the ground and the lower atmosphere, such as air flowing over topographic irregularities, is referred to as *boundary layer seeing*. Hereafter, we will often refer to the joint effect of ground surface layer and boundary layer turbulence as boundary layer seeing. The thickness of the boundary layer varies between 200 and 2000 m, depending on the local topography, latitude, wind velocity, amplitude of the diurnal thermal cycle and other environmental parameters. Katabatic flows — winds associated with the

downhill flow of colder air from mountain tops — can be considered a subset of the boundary layer component. They primarily affect locations on the slopes and near the foot of substantial peaks. Finally, the contribution to seeing of that part of the atmosphere which is above the boundary layer, in which air flow is generally almost laminar, will be referred to as *free atmosphere seeing*.

4.2. Differential Image Motion and Seeing

Our seeing measurements are carried out with a device known as *Differential Image Motion Monitor* (DIMM). It measures wavefront slope differences between two pupils on a common telescope mount, as described by Sarazin & Roddier (1990). We have deployed two DIMMs in Atacama. The first was obtained on loan from the European Southern Observatory (hereafter DIMM–4, as referred to at ESO), thanks to the kind disposition of Marc Sarazin and Riccardo Giacconi. The second was assembled at Cornell University (hereafter DIMM–C1). They each consist of of an 11–inch Celestron (C11) telescope, an SBIG ST5 CCD camera, control equipment, an aperture mask and a laptop computer equipped with specialized software written by Peter Wood and ported to ST5 by Marc Sarazin. The aperture mask is placed at the entrance pupil of the telescope and consists of two holes, 8 cm in diameter each, with centers separated by 19.2 cm. The light through one of the holes is deflected by a wedge lens, so that a stellar wavefront produces two images in the focal plane of the telescope. The two visible images (camera response peaks at $0.5 \mu\text{m}$) are recorded by the CCD camera (pixel size $10 \mu\text{m}$, corresponding to $0.74''$ at $f10$) in frames taken in succession at the maximum rate allowed by the camera electronics, i.e. about once per second. The exposure time of each frame alternates between 10 and 20 msec. As turbulent eddies cross the line of sight of the stellar source, the two images move differentially as the optical paths through the two apertures sample different sections of the wavefront, with a separation which is commensurate with r_{\circ} . On the other hand, tracking errors and wind buffeting of the telescope assembly affect equally the motion of the two stellar images in the CCD field. The fluctuations in the differential motion of the two images are related to r_{\circ} as follows.

Let d be the separation between the two holes and D the diameter of each hole. Image motion due to turbulence arises from the corrugation in the wavefront, as it reaches the aperture mask: the normal to the wavefront surface is the instantaneous angle of arrival. The covariance of the fluctuations of the angle of arrival can be related to the wavefront phase error fluctuations and, consequently, to the index of refraction structure parameter defined in the previous section, as discussed by Sarazin & Roddier (1990). The covariance in the fluctuations of the angle of arrival can be converted to a variance in the image motion, which along the direction connecting the two apertures (longitudinal) is shown by Sarazin & Roddier to be

$$\sigma_l^2 = 2\lambda^2 r_{\circ}^{-5/3} [0.179D^{-1/3} - 0.097d^{-1/3}] \quad (8)$$

while the variance in the orthogonal (transverse) direction is

$$\sigma_t^2 = 2\lambda^2 r_{\circ}^{-5/3} [0.179D^{-1/3} - 0.145d^{-1/3}] \quad (9)$$

Here, lengths are in cm and units of σ are seconds of arc. If the observations are made at a zenith angle ZA , the full width at half maximum of the stellar image can be obtained independently from Equation 8 ($i = l$ below) and Equation 9 ($i = t$ below), as discussed in the mentioned source:

$$\theta_{fwhm} \propto \lambda^{-1/5} [\sigma_i^2 \cos(ZA)]^{3/5} \quad (10)$$

The variance of the image motion is obtained from N short exposures, separately for the 10 msec and the 20 msec series (10 and 20 msec exposures are taken alternately). Since the statistical properties of the atmosphere do not change significantly over time scales on the order of 1–2 minutes, the θ_{fwhm} can be averaged over a fairly large number N of exposures of each series. We thus can obtain seeing estimates derived from 10 msec exposures, from 20 msec exposures (which typically yield lower values of θ_{fwhm} because the image motion has been smeared by the longer exposure) and extrapolations to “zero exposure”, obtained by multiplying the 10 msec seeing by the ratio of the 10 and 20 msec measurements. This is based on the results of Martin (1987), where it is shown that for experimental configurations such as ours, the variation of the attenuation of the variance with exposure time is close to exponential. If we assume that $\sigma^2(t) = \sigma^2(0)e^{-at}$, measurements at t and $2t$ can be combined to obtain $\sigma(0) = \sigma(t)[\sigma(t)/\sigma(2t)]$. In the unusual instance in which the 10 msec θ_{fwhm} is smaller than the 20 msec θ_{fwhm} , for the zero exposure θ_{fwhm} we take the average of the two nonzero exposure measurements. In the next Section, we will present statistics for the three exposure times separately, for ease of comparison with monitors that measure image motion at a fixed exposure time.

The technique assumes that the perturbed wavefront is swept across the aperture in its frozen form during the exposure (“Taylor’s hypothesis”). Since *differential* image motion is recorded by the DIMM, the instrument does not sense turbulent eddies much larger than d , which produce the same distortion over the two apertures. The differential image motion is thus determined by the flow, at the wind speed, of small-scale eddies, which takes place on short time scales. If w is the wind velocity at the perturbing layer, ideally the exposure time should then be $\ll d/w$; practical limitations are imposed by the clock resolution of the CCD and the necessity to detect enough photons so that centroiding of the stellar image is reliable with readily observable stars at any time. Note that an eddy of $r_o = 20$ cm ($\theta_{fwhm} = 0.5''$ at $\lambda = 0.5 \mu\text{m}$) will cross the line of sight in 20 msec, in a 10 m sec^{-1} wind. Alternating exposures of 10 and 20 msec, it is possible to obtain an indication on how far the atmosphere departs from the assumption mentioned above, and extrapolate to infer an approximation of the ideal case of “zero exposure seeing”. The accuracy of the final seeing figure depends on N , d , D , r_o , the stability of the atmosphere and the precision of the instrumental setup, mainly the telescope focus which also determines the scale of the image in the focal plane.

As mentioned above, differential image motion is insensitive to turbulent scales significantly larger than d . This may introduce a bias in carrying the seeing estimates inferred from a DIMM to those expected for a large telescope of diameter close to the upper limit of the Kolmogorov inertial range. It appears clear now that a finite outer scale L_o of turbulence exists, varying principally

between 10 and 25 m (Martin et al. 1999; Avila 2000; Bouzid 2000; Linfield et al. 2001), which is commensurate with the size of large telescopes. In fact, the seeing at the VLT is often significantly better than that obtained by a DIMM next to the telescope; that difference is 10% in the optical and even more in the NIR (Sarazin, personal communication).

From Sarazin & Roddier (1990), the error in the measurement of the image motion variance is given by

$$\frac{\delta\sigma_i^2}{\sigma_i^2} \simeq \sqrt{\frac{2}{N-1}} \quad (11)$$

which can be converted to an error on θ_{fwhm} via equation 10:

$$\frac{\delta\theta_{fwhm}}{\theta_{fwhm}} \simeq \frac{3}{5} \sqrt{\frac{2}{N-1}} \quad (12)$$

In mild wind conditions and for $r_o < 40$ cm ($\theta_{fwhm} > 0.25''$) errors on θ_{fwhm} smaller than 10% can be obtained from the DIMM, by averaging $N \sim 100$ exposures. The instrumental setup does however rapidly lose accuracy for $r_o > 40$. Martin (1987) has investigated thoroughly the accuracy of seeing derived from the differential image motion technique.

We average seeing measurements over intervals of up to 8 minutes in time ($N \sim 100$), providing a seeing figure to compare with those of astronomical imaging exposures of typical duration. Independently, longitudinal and transverse image motion is monitored and seeing derived from each; we verify that the two indications yield statistically the same seeing and then averaged together. All seeing figures mentioned in this report refer to a wavelength of $0.5 \mu\text{m}$ and are corrected to a zenithal line of sight. Both DIMM telescopes were mounted on a rigid platform which elevated the aperture to approximately 2.5 m above the ground. Every time measurements were made, the DIMMs were in thermal equilibrium with the ambient air.

4.3. Instrument Comparison

Comparisons were made between DIMM-4 and DIMM-C1 for two nights. The results of the two were identical to within the measurement errors, as should be expected because both the hardware and the software of the two devices are identical. More important was the comparison carried out during two nights in October 2000 between DIMM-C1 and a DIMM brought to Atacama by a Cerro Tololo Interamerican Observatory team (R. Blum, M. Boccas, E. Bustos and B. Gregory). The CTIO DIMM had a higher data rate but it only integrated at one exposure time, which was set to 20 msec on the first night and to 10 msec on the second. The seeing measurements could thus be compared between the two devices, which were different in both hardware and software. Figure 5 illustrates the comparison of the two sets of data. The two devices were placed to within 10 m of each other, at the summit of Cerro Honar, at 5400 m. The aperture of the CTIO DIMM was closer to the ground (approximately 1 m) than DIMM-C1 (approximately 2.5 m); both were within 5 m

of the mountain edge, in the direction of the incoming wind. A wind screen of negligible thermal capacity protected the CTIO DIMM; no screen protected DIMM–C1, which was more vulnerable to wind shake; this produced numerous interruptions of data taking and consequent reduction in the number of averaged records N and increased error in the DIMM–C1 measurements. The comparison between the two data sets reveals no noticeable bias and good agreement to within the expected errors. The split between the 10 msec and 20 msec seeing values is due in part to the fact that conditions were better during the night of 20 msec comparison, and in part to the fact that 20 msec exposures smear image motion and produce lower seeing values than those derived from image motion obtained from shorter exposures, as discussed in the preceding Section.

4.4. Measurement Strategy and Routines

The ultimate purpose of our measurements is to establish the statistical properties of θ_{fwhm} at the best sites in the National Science Preserve region in the Atacama. A number of constraints are imposed on our campaign strategy. Given the high altitude and budgetary restrictions, it is impractical to consider *extended* measurement campaigns on summits to which vehicular access is currently impossible. While the construction of a robotic DIMM is now under way in Ithaca, obtaining a device that will work reliably and unattended at a remote site requires extensive testing and substantial resources. A robotic device will also be less portable, so its use should be aimed at testing the long term characteristics of a well chosen site.

Transportation of equipment and power sources restricts the ability to perform measurements to locations on the plateau and to a few elevations surrounding them. The latter include (a) two locations (one on Cerro Toco and one on Cerro Chajnantor) at which now abandoned sulphur mines were operated in previous decades, (b) the summit of the chain of Cerros de Honar, to which we have recently opened a rudimentary access road and (c) Cerro Chico, to which a small communications repeater was installed by a gas pipeline construction company. Access can be negotiated with rental four-wheel drive vehicles to those four locations. Those in Toco and Chajnantor, however, do not lead to prime locations for seeing measurements: neither reaches the summit and, in both cases, the track is on the east side, and thus on the prevailing wind shadow of the mountain mass. In addition to strong disturbances in the air flow produced by that circumstance, katabatic winds are also a concern in those two cases. For Cerro Chico and Cerros del Honar, however, vehicular access to the summits is possible. Both have a relatively clear immediate western horizon, although Cerro Negro and Cerros de Macón, almost as high as Chico and only 300 m lower than Honar, are a few km away in the direction of prevalent incoming winds. Moreover, Chico is located only 2 km from the foot of Cerro Chajnantor, and the effect of katabatic winds from Chajnantor, a significantly more substantial and higher mountain mass, is a concern. Access to the other summits (Chajnantor, Toco, Negro and Chascón) at this time requires foot hikes several hours long. The construction of even a rudimentary drivable track to any of those summits would be expensive, as would the transportation of equipment by means of a helicopter suited for high altitude flight.

Given the aforementioned circumstances, a seeing campaign strategy was developed that would follow three phases:

I. We would first establish a reference frame for seeing statistics in the region at an easily accessible site, possibly above the local boundary layer. We would determine reliably the site’s average seeing properties and seasonal variations, by carrying out a series of seeing runs spread over the seasonal cycle. This phase requires the deployment of a single DIMM (DIMM–4).

II. Next, we would compare characteristics of potentially attractive sites by means of relatively brief runs of seeing measurements at those sites, simultaneous with measurements at the reference site. This phase requires the deployment of two DIMMs (DIMM–4 and DIMM–C1)

III. Finally, once the site with the best comparative characteristics is identified, a long–term campaign of continuous monitoring with a robotic DIMM would be carried out. This phase requires the deployment of a robotic DIMM, currently under construction.

Given its accessibility, possible partial emergence above the atmospheric boundary layer and central location in the Science Preserve Area, we chose Cerro Chico as the site at which a seeing reference standard for the region would be established (the road to Honar was not completed until August 2000). Observing consisted of runs of 8–10 days duration each, spaced by approximately two months. Seven such runs have been carried out, sufficient to fairly characterize the seeing at Chico. This series of runs was preceded by a single run at the plateau level in May 1998, in the course of which DIMM–4 was deployed at the NRAO testing site (“ALMA container”, position of label 2 in Figure 2), at an elevation of 5050 m. This decision was made in order to ascertain our and the equipment’s ability to effectively function at high altitude. Caution advised that such verification be made near a shelter. Successively, runs were carried out at the summit of Cerro Chico, some 2 km NW and about 100 m higher than the ALMA container. A list of the runs and their durations is given in Table 1. Columns 1 and 2 list the date of each run and the location; column 3 lists the number of nights (N_n) and the number of hours (N_h) in which useful data were collected; columns 4–12 list the 25%, 50% and 75% quartile values of θ_{fwhm} , measured respectively for the extrapolated “zero exposure seeing” (cols. 4–6), the 10 msec exposures (cols. 7–9) and 20 msec exposures (cols. 10–12). The coordinates of the two sites are given in Table 2. Atacama is in the Universal Transverse Mercator (UTM) zone nr. 19.

During operation, the DIMM aperture stands some 2.5 m above the ground. During the May 1998 run, the DIMM was placed about 5 m away from the shipping container that serves as shelter for NRAO’s ALMA monitoring station. During observations, the DIMM was always upwind from the container. During the observations at Chico, the DIMM was placed on the summit of this modest orographic formation, at less than 5 m from its western edge, which slopes downhill rather steeply in the prevailing direction of incoming winds. This choice was motivated by the results of the simulations by De Young & Charles (1995) of airflow over telescope sites, and the experience of ESO at Paranal and La Silla, which indicates that the effect of ground layer turbulence can be minimized by placing the DIMM near the edge of a summit, facing the incoming direction of

prevailing winds. According to Martin et al. (2000), the median contribution to the seeing of the ground boundary layer, between 2 m and 21 m above the ground, is 7% of the total, with most of it occurring between 2 and 7 m. For a median seeing near $0.7''$, the contribution of the ground boundary layer alone would be on the order of $0.25''$, assuming that each layer’s contribution adds quadratically. Given our telescope setup, some measure of degradation of the seeing due to ground boundary layer should then be expected. In normal conditions, such deterioration is probably below the 10% level. During exceptionally good nights, however, the effect of the ground boundary layer may be more important.

During measurements, we power the DIMM hardware off a regular automobile battery, which is charged daily by connecting it to the engine of a vehicle. Each evening after sunset, telescope setup takes approximately 30 minutes. Each observing shift involves two persons. A first or second magnitude star is acquired, preferably to the south of zenith, so that the tracking errors resulting from misalignment between the telescope’s and the Earth’s polar axis are minimized. No more than 2 target stars per night are necessary; they are tracked at air masses generally between 1.1 and 1.6. Automatic guiding is provided by the DIMM software, and in routine operation, no attention is required, except for the impact of exceptional environmental effects (wind gusts, frost forming on the telescope mask, etc.) or occasional electronic glitches. DIMM data consists of a time series of (a) image motions, both longitudinal and transverse to the direction of the axis of the two holes in the mask; these are converted to seeing figures via Equation 10; (b) a scintillation index, which is the variance of the flux associated with each image; (c) time, zenith angle, focus, image scale and ancillary instrumental parameters. Roughly one record per second is acquired. Exposures of 10 msec and 20 msec are taken alternately, and separately analyzed. Off-line, the data is extrapolated to “zero exposure”, as described in the preceding section, and averaged over intervals of between 2 and 8 minutes.

4.5. Seeing Measurements: Results

Figure 6 displays time series of “zero exposure seeing” data for each day of the December 1998 run. Similar plots for the other runs can be seen in <http://www.astro.cornell.edu/atacama>. Solid symbols identify 8 minute seeing averages on Cerro Chico, while the horizontal dashed lines indicate the daily median seeing. The thin solid line in each panel is a running mean of the Cerro Paranal seeing measurements obtained with a DIMM similar to DIMM-4, at the same time as our data. Note that local midnight is at $UT = 4.5^h$.

As illustrated in Table 1, the statistical properties of each of the Cerro Chico runs are rather similar. The median values of the 0 ms seeing vary between $0.65''$ and $0.76''$, those of the 10 msec seeing between $0.56''$ and $0.65''$ while those of the 20 msec seeing between $0.48''$ and $0.56''$. Quartiles of $0.56''$, $0.71''$ and $0.87''$ for the overall data set, including 38 nights and 153 hours of data, appeared to be closely mimicked by the corresponding values for each run. In contrast, the May 1998 run at the plateau level gave significantly higher quartile values of $0.93''$, $1.09''$ and $1.28''$.

Figure 7 displays a comparative summary of the seeing measurements at the ALMA container and at Cerro Chico. The distributions for the two sites are significantly different. It should be remarked that the Cerro Chico and ALMA container measurements are not simultaneous.

The seeing at the beginning of the evening tends to be of lower quality. Such measurements are generally made still in twilight conditions, as there are advantages to doing the telescope setup in sunlight. The observation of significant improvement occurring 1–2 hours later is also a common experience. This effect appears to be correlated with a decrease in the wind speed, which as we have seen usually occurs 1–2 hours after sunset. The second part of the night tends to have better seeing than the first; yet, the larger fraction of Cerro Chico data correspond to the first half of the night.

Some data exist of simultaneous seeing and precipitable water vapor measurements. The latter are discussed in Paper II. Eight reliable simultaneous measurements are currently available. Of those, the four with total precipitable water vapor $PWV < 1$ mm correspond to an average seeing of $0.51''$ at $0.5 \mu\text{m}$, while the other four, with $PWV > 1$ mm, correspond to an average seeing of $0.84''$. For the first set of four, the water vapor layer was tightly packed at low altitudes above the ground, 50% of PWV being in each case contained within 500 m from the plateau level. For the second set of measurements, those with high PWV, the water vapor was distributed more widely in the vertical direction, the 50% boundary being above 1000m in each case. This correlation is suggestive but statistically still quite weak.

While there should be no expectation for Cerro Chico to deliver the best seeing in the National Science Preserve region, it is useful to compare it to other prime astronomical sites. The established astronomical site with the best historical seeing record, as measured with a similar technique to our own is Cerro Paranal. Cerro Paranal boasts a “zero exposure seeing” median of $\theta_{fwhm} = 0.66''$, over several years of systematic DIMM tests (see <http://www.eso.org/gen-fac/pubs/astclim>). The historical median at La Silla, by comparison, is $0.87''$. The La Silla and Paranal measurements were obtained with a DIMM analogous to the one we used in Chajnantor and similarly calibrated. Cerro Paranal is located some 250 km to the west and 180 km to the south of the Llano de Chajnantor. Figure 8 shows a comparison of the seeing statistics for Cerro Chico and Cerro Paranal, for 34 simultaneous nights of observations. Cerro Chico’s seeing ($\theta_{fwhm} = 0.71''$) is about 12% better than that at Paranal ($\theta_{fwhm} = 0.80''$). During the period of these measurements, however, Cerro Paranal’s seeing was about 21% worse than its historical median. This circumstance has been noted by Sarazin & Navarrete (1999), and ascribed to the exceptional *El Niño/La Niña* anomaly discussed in Section 3, which should have affected the Chico seeing as much as it affected Paranal’s. There has been an improving trend in the Paranal seeing in the last few months of 2000, bringing it to match its historical performance. Such an improvement was not noticeable at Chico, at least for the limited duration of the October 2000 run.

5. Photometric Conditions

We have not conducted a strict, quantitative survey of the photometric conditions at Chajnantor. We have however kept a visual record of the sky conditions, based on the substantial, combined experience of participants at the seeing runs and anchored by the individual estimates of RG, who took part in all the runs. Of the 84 nights with good visual records, 53 (63%) were deemed photometric, 15 (18%) were not photometric, with partial cloudiness, but suitable for other astronomical work, and 16 (19%) were more than 60% overcast. This included a full run of 11 cloudy nights (March 1999).

This record of observations yields a lower fraction of clear nights than obtained from historical satellite data records by Erasmus (2000), whose results based on 6.7 μm GOES 8 satellite imagery indicate that the atmospheric layers above 7500 m altitude in the Chajnantor region were clear of clouds (cloud cover less than 70% of sky) more than 90% of the time between January 1995 and February 1996. The disparity between our visual record and the Erasmus’ results may reflect the *El Niño/La Niña* anomaly of 1998, the contribution of low lying clouds to sky cover, or poor statistics for our visual records. At any rate, it is unlikely that the fraction of photometric nights at Chajnantor can match the extraordinary record of Cerro Paranal.

6. Discussion and Future Work

We have obtained a reliable reference frame for measurements of seeing in the Chajnantor region. Provided by observations at Cerro Chico over 38 nights spread over the seasonal cycle, this reference frame is currently being used to compare different sites in the vicinity of the Llano de Chajnantor. While Cerro Chico does not qualify as a site expected to deliver the best observing conditions among astronomically attractive sites in the region, it has easy access, it produces results with repeatable statistics and is thus a good choice for benchmarking quality comparisons through simultaneous measurements at different sites. It also turns out to deliver high quality seeing, comparable with that of some of the best observatories on Earth. This allows for good expectations for the quality of other sites in the region. The next phase of our campaign involves a series of runs of simultaneous seeing measurements at Chico and other summits, in the course of which we will learn the differential qualities of the various sites, and we will be able to tie those to the increasingly more robust data sample for Cerro Chico itself.

The difference between the seeing measurements at the ALMA Container and at Cerro Chico, a mere 100 m above the plateau level, suggests that boundary layer contributions dominate seeing at the plateau. This result was partly expected, for air flow at the plateau level is strongly influenced by thermally driven effects which, during daytime, result in strong winds from the west and, during quiescent nights, in katabatic winds off the surrounding mountain slopes. As expressed by the Richardson number, the onset of turbulence depends on the temperature gradient and the wind shear: the inhibition of convection produced by the positive thermal gradient with increasing

altitude normally occurring at night in the lower 100 m of the atmosphere (Figure 3), is counterbalanced by strong wind shear (Figure 4). While the derivation of C_n^2 from the coarse median profiles shown in Figures 3 and 4 is impossible due to their low resolution, it is well known (Hufnagel 1978) that the occurrence of temperature inversion layers in the troposphere tends to be accompanied with increased C_n^2 just below the inversion. While a good fraction of the boundary layer seeing clearly arises from the lowest 100 m over the plateau, as the comparison of the seeing measured at the ALMA Container and at Cerro Chico shows, an important fraction of it probably originates above the summit of Chico, for inversion layers between 200 and 1000 m above the ground are common, as shown by radiosonde data in Paper II. Thus, optimistic expectations for high quality seeing at higher altitude peaks in the region are justified.

The free atmosphere seeing arises mostly from temperature fluctuations associated with the tropopause and the jet stream; the median value of θ_{fwhm} has been estimated to vary between 0.31" at La Silla, 0.37" at the South Pole, and 0.40" to 0.46" at Mauna Kea, La Palma and Paranal. As for the boundary layer, Marks *et al.* (1999) give estimates of its thickness at various astronomical sites. They range between 220 m at the South Pole, 900 m at La Silla and 2000 m at Cerro Paranal. At the Llano de Chajnantor region, the combination of ground surface layer and orographic boundary layer seeing may be quite complex: while the mean ground level rises gradually but steeply between the 2300 m of the Salar and the 5000 m of the plateau to the east, several hill formations stand between them, reaching elevations of about 5000 m (Cerro Negro and Cerros de Macón). Their influence on the thermal stability of the air flow is likely to be important, and dependent on the specific direction of the wind. A study of the characteristics of the air flow in the region by means of computer simulations is being carried out by D. De Young.

At this stage, a few simple considerations can be made regarding expectations for potentially interesting sites in the region: (i) it is likely that by accessing higher sites, the quality of the seeing will improve, with respect to the already excellent values measured at Cerro Chico; (ii) the infrared transparency improves with elevation, as discussed in Paper II; (iii) such improvements will come with disadvantages, mainly that associated with progressively increasing high altitude discomfort and rapidly increasing wind speeds, which will place a burden on construction and operation of telescopes. The candidate sites for future testing include the summit of the Honar chain, Cerro Toco, Cerro Chajnantor, Cerro Chascón and Cerro Negro. Measurements at Honar are already under way.

The current, preliminary conclusions on the seeing conditions in the Chajnantor region are as follows:

- The median seeing at 0.5 μm over 7 nights, at the plateau level of 5050 m, is $\theta_{fwhm} = 1.1''$. This is strongly affected by boundary layer contributions.
- The optical seeing measured at Cerro Chico, 100 m above the plateau level is $\theta_{fwhm} = 0.7''$ over 38 nights, between July 1998 and October 2000; this is 12% better than the seeing at

Cerro Paranal. This result is likely to be an overestimate of the historical median for Cerro Chico, as in the same period the seeing at Paranal was 21% higher than its historical median.

- The percentage of optically photometric nights over the Chajnantor region is near 60%, while that of nights useful for astronomical observations is close to 80%.
- Cerro Chico can now provide a benchmark against which to test the quality of other sites in the region, via dual, simultaneous seeing measurements. Such efforts are under way.

Acknowledgments: The support of Don Randel, Yervant Terzian, Joseph Veverka and Bryan Isacks of Cornell University, Riccardo Giacconi, Angel Otarola, Peter Shaver and Alvio Renzini of ESO, Martha Haynes of Cornell and Associated Universities, Inc., Robert L. Brown, Eduardo Hardy, Simon Radford and Geraldo Valladares of NRAO, don Tomás Poblete Alay and the staff of *La Casa de Don Tomás* are thankfully acknowledged. This study was made possible by a grant of the Provost’s Office of Cornell University and a National Science Foundation grant AST–9910136.

REFERENCES

- Avila, R. 2000, in *Astronomical Site Evaluation in the Visible and Radio Range*, Marrakech. Proceedings being edited by J. Vernin, M. Sarazin & Z. Benkhaldoun
- Bouزيد, A. 2000, in *Astronomical Site Evaluation in the Visible and Radio Range*, Marrakech. Proceedings being edited by J. Vernin, M. Sarazin & Z. Benkhaldoun
- Cook, K. 2000, paper presented at the *Atacama Telescope Workshop*, Cornell University, Ithaca, NY.
- De Young, D.S. & Charles, R.D. 1995, AJ 110, 3107
- Erasmus, A. 2000, in *Astronomical Site Evaluation in the Visible and Radio Range*, Marrakech. Proceedings being edited by J. Vernin, M. Sarazin & Z. Benkhaldoun
- Fuenzalida, H. 1984, in *Site Testing for Future Large Telescopes*, ed. by A. Ardeberg & L. Woltjer, ESO:Garching
- Gardeweg, M.C. 1996, MMA Memo Series nr. 251
- Giovanelli, R., Darling, J., Stacey, G., Henderson, C., Hoffman, W., Cordes, J., Eikenberry, S., Gull, G. 2001, preprint.
- González–Ferràn, O. 1994, *Volcanes de Chile*, Instituto Geográfico Militar: Santiago
- Hufnagel, R.E. 1978, in *The Infrared Handbook*, ed. by W.L. Wolfe & G.J. Zissis (U.S. Govt. Printing Office: Washington, D.C.), Chapter 6.

- Linfield, R.P., Colavita, M.M., & Lane, B.F. 2001, astro-ph/0102052
- Marks, R.D., Vernin, J., Azouit, M., Manigault, J.F. & Clevelin, C. 1999, *Astron. & Astrophys. Suppl. Ser.* 134, 161
- Martin, F., Conan, R., Tokovinin, A., Ziad, A., Trinquet, H., Borgnino, J., Agabi, A. & Sarazin, M. 2000, *A&A Suppl. Ser.* 144, 39
- Martin, H.M. 1987, *PASP* 99, 1360
- McPhaden, M.J. 1999, *Science* 283, 950
- Radford, S. 2000, in <http://www.tuc.nrao.edu/mma/sites/Chajnantor>
- Roddier, F. 1981, *Prog. Opt.* 19, 281
- Sarazin, M. & Navarrete, J. 1999, *ESO Messenger* 97, September 1999, p. 8
- Sarazin, M. & Roddier, F. 1990, *A&A* 227, 294
- Schmidt, D. 1996, *Das Extremklima der Nordchilenischen Hochatacama Unter Besonderer Berücksichtigung der Höhengradienten*, Ph. D. Thesis, Friedrich–Alexander–Universität Erlangen–Nürnberg.
- Tatarski, V.I. 1961, *Wave Propagation in a Turbulent Medium*. McGraw–Hill, New York.
- Tokunaga, A.T. 1998, in *Astrophysical Quantities*, 4th edition, editor A. Cox, Springer–Verlag, in press.

Table 1. Seeing Data Summary

Date	Location	N_n/N_h	0 ms			10 ms			20 ms		
			$\theta_{25\%}$	$\theta_{50\%}$	$\theta_{75\%}$	$\theta_{25\%}$	$\theta_{50\%}$	$\theta_{75\%}$	$\theta_{25\%}$	$\theta_{50\%}$	$\theta_{75\%}$
May98 ¹	ALMA	5/41	0.93	1.09	1.28	0.85	0.97	1.12	0.72	0.81	1.00
Jul98 ²	Chico	3/14	0.53	0.66	0.75	0.47	0.59	0.67	0.39	0.49	0.59
Oct98	Chico	7/33	0.52	0.70	0.86	0.46	0.59	0.73	0.39	0.48	0.64
Dec98	Chico	7/31	0.50	0.66	0.90	0.44	0.56	0.75	0.38	0.48	0.66
Mar99 ³	Chico	1/2		0.70							
Apr00	Chico	9/28	0.59	0.72	0.80	0.54	0.64	0.77	0.48	0.56	0.67
Jul00 ⁴	Chico	2/4	0.44	0.65	0.85	0.40	0.60	0.75	0.36	0.55	0.75
Oct00	Chico	9/41	0.59	0.76	0.93	0.53	0.65	0.77	0.46	0.56	0.68
All	Chico	38/153	0.55	0.71	0.87	0.49	0.61	0.75	0.42	0.52	0.66

N_n, N_h are the total nr of nights, of hours observed.

¹Three nights lost to bad weather.

²Data taking limited by equipment malfunction.

³Bad weather for full run duration: Bolivian Winter conditions.

⁴Data loss due to bad weather; data of dubious quality taken 3 other nights.

Table 2. Site Coordinates

Site	Latitude	Longitude	UTM Northing	UTM Easting	Elevation
ALMA Container	S 23° 01'.2	W 67° 45'.2	7453.7 km	627.8 km	5050 m
Cerro Chico	S 23° 00'.3	W 67° 46'.3	7455.7 km	626.2 km	5150 m

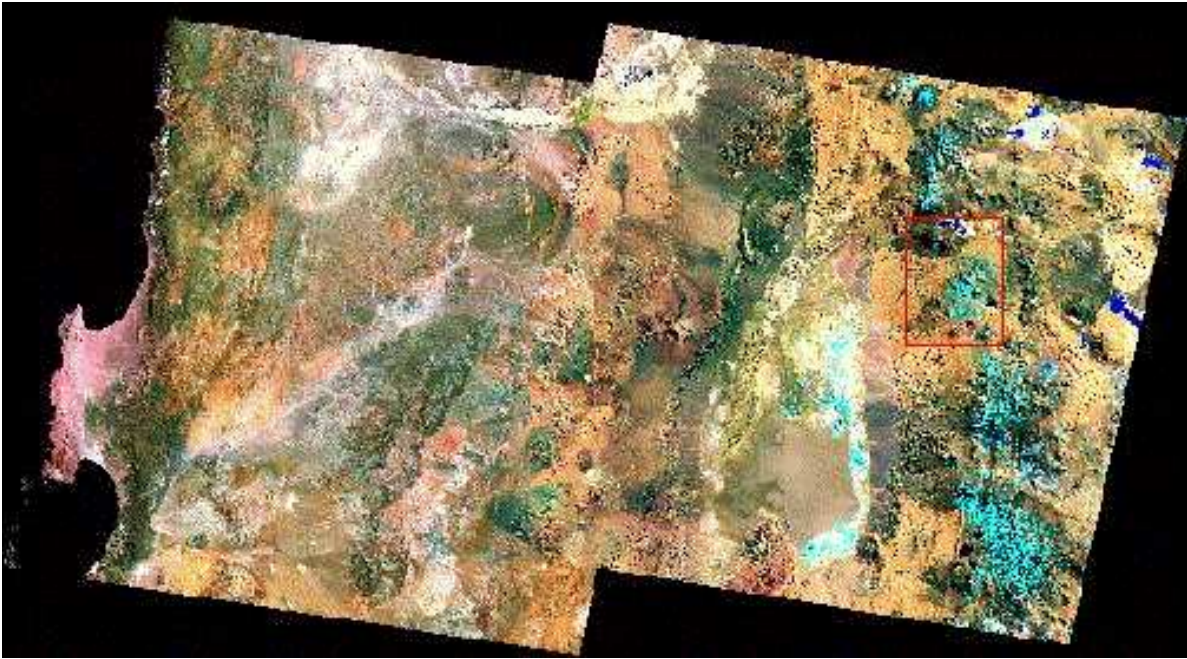


Fig. 1.— Satellite composite view of the Atacama region. The image encloses a region of approximately 400 by 200 km, extending from the Pacific coast to the West (left) to the Andean divide to the East. The city of Antofagasta is just to the South of the anvil shaped Mejillones Peninsula. Calama and Chuquicamata are located slightly North of the center of the image, while the Salar de Atacama is the brown region to the SE of center, bordered on its eastern side by light blue hues. The red square box is centered on the Chajnantor Plateau, better seen in Figure 2. The NE side of the image includes Bolivian territory; Argentina is just off the eastern (right) edge.



Fig. 2.— Satellite composite view of the Chajnantor Plateau region. The image subtends an area of approximately 1500 square km. North is up and left is West. It corresponds roughly to the region within the red outline in Figure 1. Labeled features are identified in Section 2.

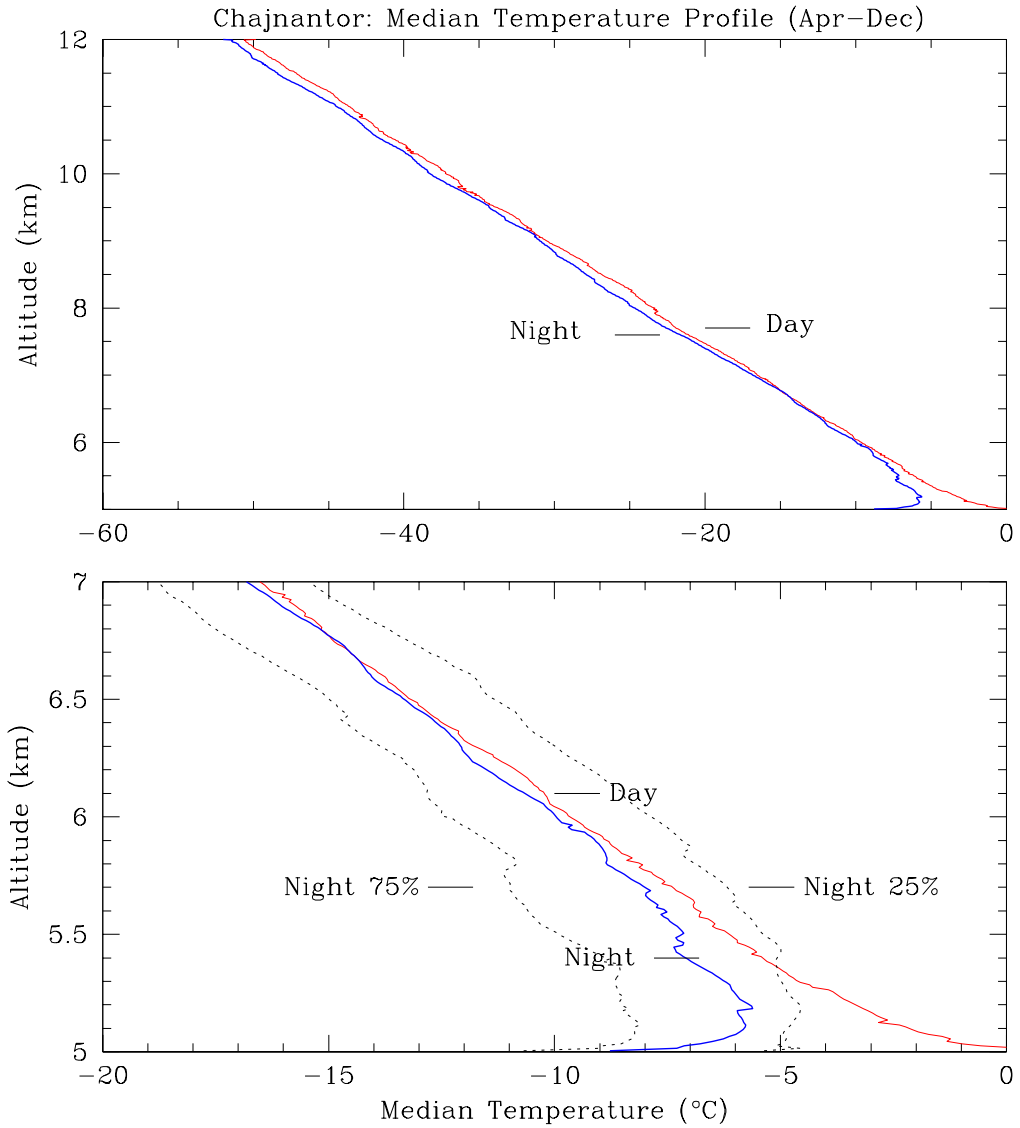


Fig. 3.— Mean Temperature profile above Chajnantor. Night profile obtained from 30 sonde flights; day profile obtained from 65 sonde flights. Dotted lines represent the 25% and 75% quartiles during night. Sondes were launched between April and December. The lower panel shows an expanded view of the lower 2 km of atmosphere.

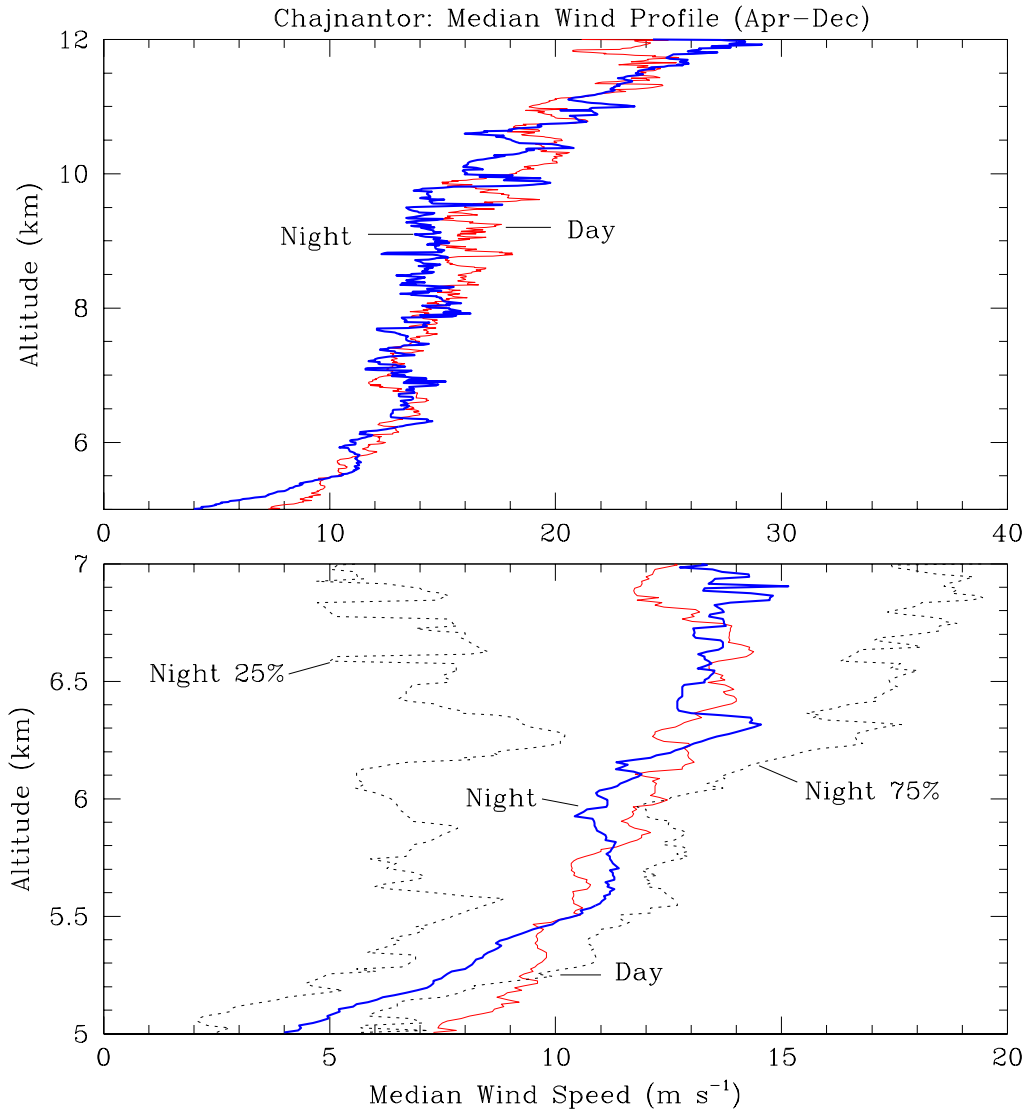


Fig. 4.— Mean wind speed profile above Chajnantor. Night profile obtained from 30 sonde flights; day profile obtained from 65 sonde flights. Dotted lines represent the 25% and 75% quartiles during night. Sondes were launched between April and December. The lower panel shows an expanded view of the lower 2 km of atmosphere.

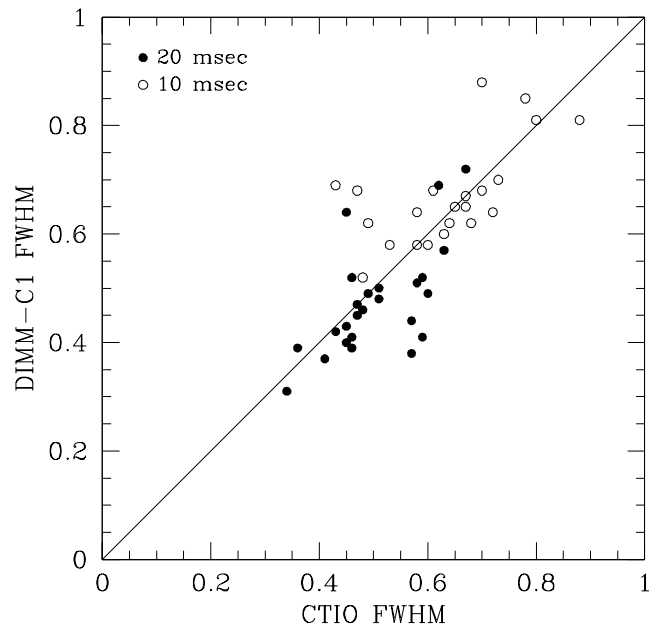


Fig. 5.— Comparison of seeing measurements carried out with DIMM-C1 and the CTIO DIMM on two nights of October 2000.

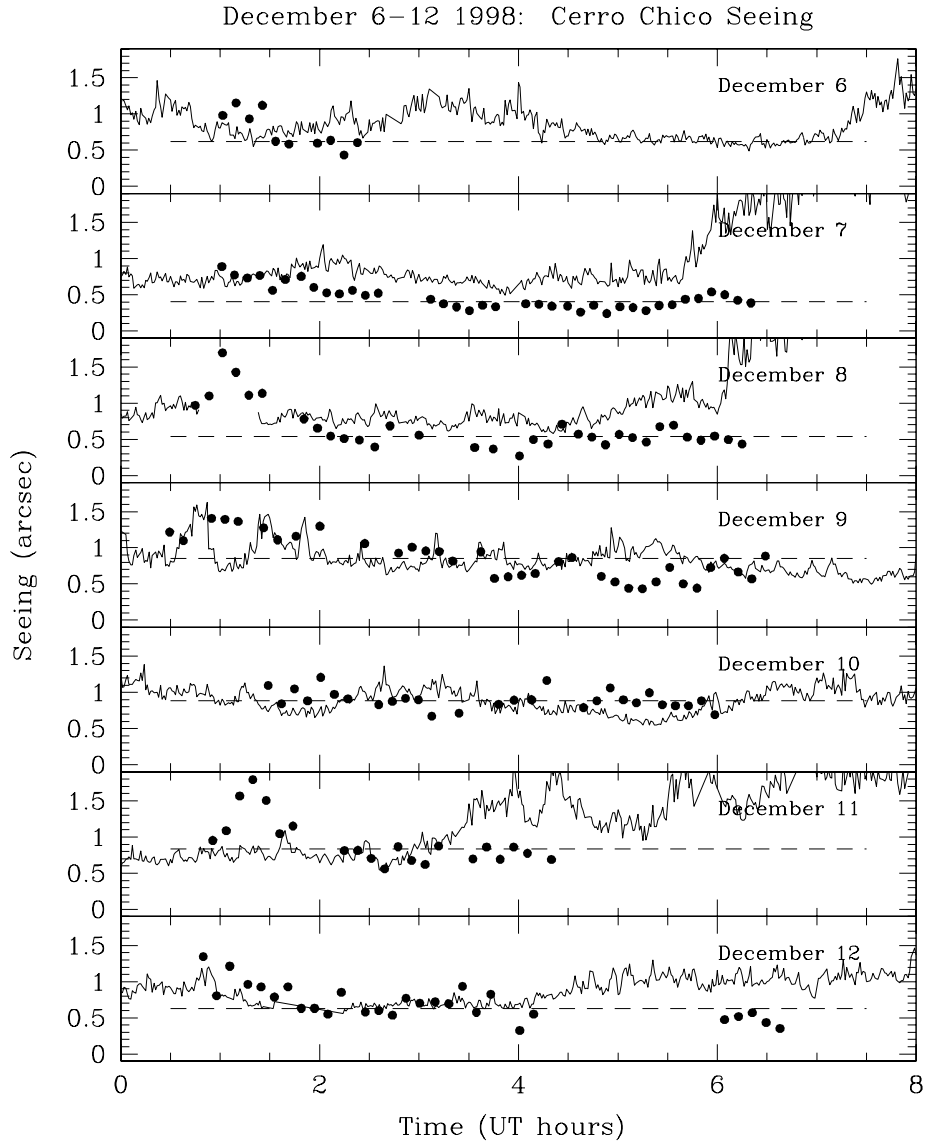


Fig. 6.— Time series of seeing measurements for the December 1998 run. Filled circles are 8-minute seeing averages at Cerro Chico; thin solid lines represent simultaneous seeing at Cerro Paranal. Dashed lines are nightly Cerro Chico medians. Analogous plots for other runs can be seen at <http://www.astro.cornell.edu/atacama/>. Local midnight occurs at 4.31^h UT.

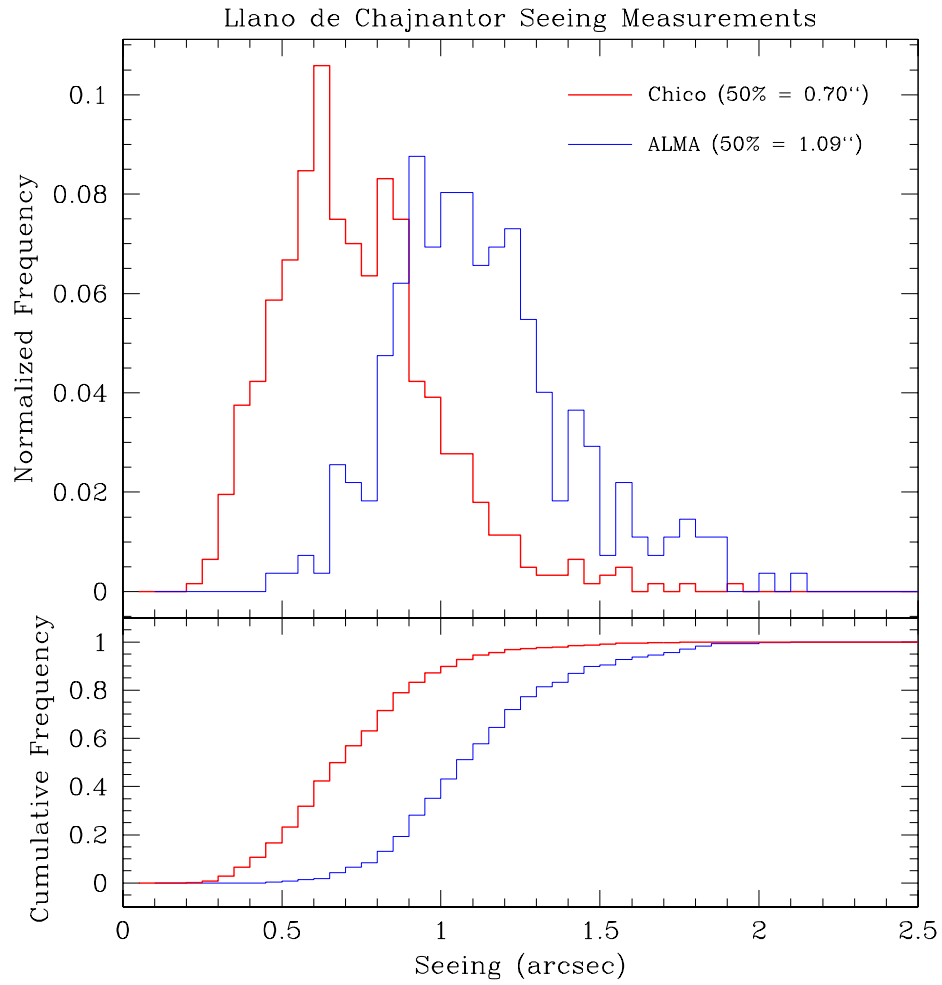


Fig. 7.— Comparison of seeing at the ALMA Container and Cerro Chico, including all of 1998 Cerro Chico runs and May 1998 ALMA run.

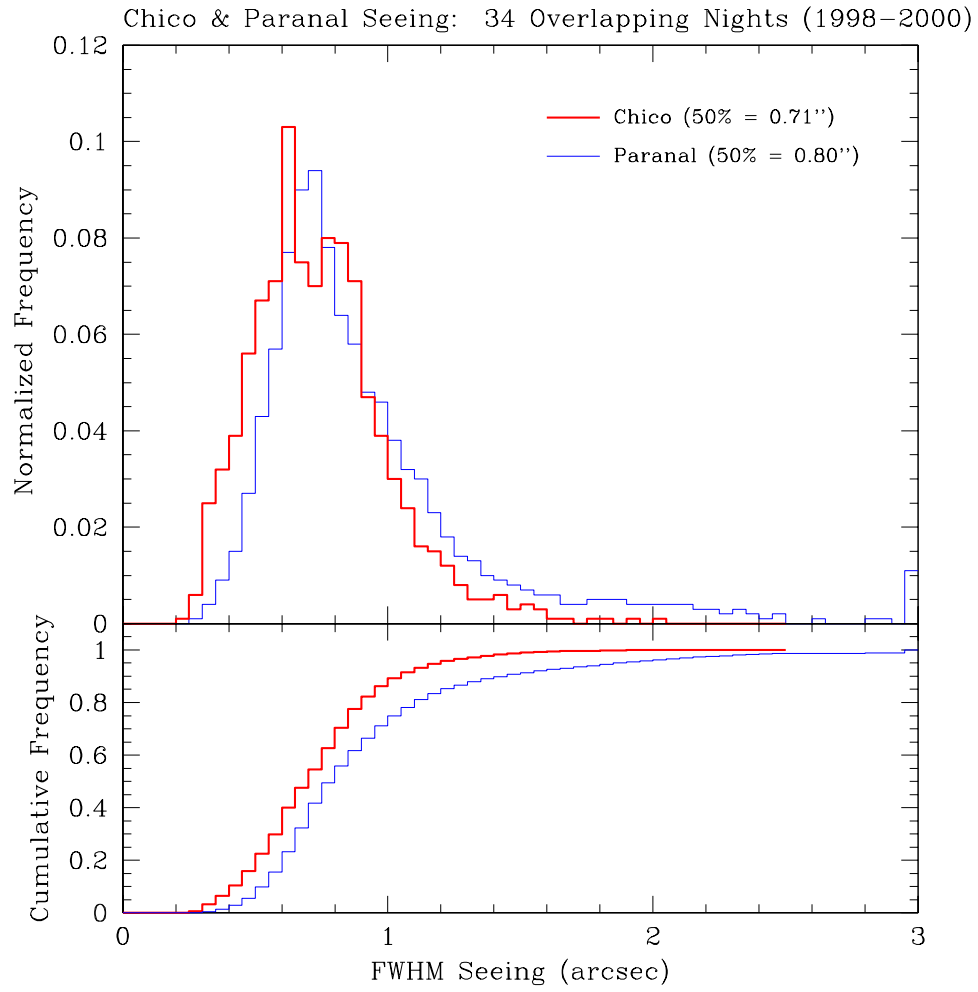


Fig. 8.— Comparison of seeing at the Cerro Paranal and Cerro Chico.